

Please cite the Published Version

Souza, MMC, Siqueira, GP, Rocha, RG, Crapnell, RD , Santana, MHP, Richter, EM, Banks, CE  and Muñoz, RAA  (2025) Additively Manufactured Collector-Detector Device for Explosive Analysis Using Recycled PLA Filament Loaded with Carbon Black and Graphite. Journal of the Brazilian Chemical Society, 36 (4). pp. 1-13. ISSN 0103-5053

DOI: <https://doi.org/10.21577/0103-5053.20240186>

Publisher: Sociedade Brasileira de Quimica (SBQ)

Version: Published Version

Downloaded from: <https://e-space.mmu.ac.uk/639387/>

Usage rights:  [Creative Commons: Attribution 4.0](https://creativecommons.org/licenses/by/4.0/)

Additional Information: This is an open access article published in Journal of the Brazilian Chemical Society, by Sociedade Brasileira de Quimica (SBQ).

Enquiries:

If you have questions about this document, contact openresearch@mmu.ac.uk. Please include the URL of the record in e-space. If you believe that your, or a third party's rights have been compromised through this document please see our Take Down policy (available from <https://www.mmu.ac.uk/library/using-the-library/policies-and-guidelines>)

Additively Manufactured Collector-Detector Device for Explosive Analysis Using Recycled PLA Filament Loaded with Carbon Black and Graphite

Maria M. C. Souza,^a Gilvana P. Siqueira,^a Raquel G. Rocha,^a Robert D. Crapnell,^b Mário H. P. Santana,^c Eduardo M. Richter,^a Craig E. Banks^b and Rodrigo A. A. Muñoz^{b,*}

^aNúcleo de Pesquisa em Eletroanalítica, Instituto de Química, Universidade Federal de Uberlândia, 38408-902 Uberlândia-MG, Brazil

^bFaculty of Science and Engineering, Manchester Metropolitan University, Manchester, M1 5GD, UK

^cUnidade Científica, Polícia Federal Uberlândia, 38408-663 Uberlândia-MG, Brazil

We report the electrochemical potential of conductive filaments produced with recycled polylactic acid (rPLA) alongside a mixture of graphite (Gpt) and/or carbon black (CB) and castor oil to create an electrode ready-to-use. Additively-manufactured electrodes (AMEs) were compared with commercial-conductive filament composed of PLA and CB. The Gpt-CB-rPLA and CB-rPLA sensors showed lower charge-transfer resistance (R_{ct}) and a greater heterogenous rate constant, k^0 , ($R_{ct} = 1040 \pm 50 \Omega$ and $1810 \pm 30 \Omega$ and $k^0 = 6.91 (\pm 0.58) \times 10^{-3}$ and $5.31 (\pm 0.40) \times 10^{-3} \text{ cm s}^{-1}$, respectively) compared to the sensor from the commercial filament ($R_{ct} = 9620 \pm 280 \Omega$ and $k^0 = 3.62 (\pm 0.38) \times 10^{-3} \text{ cm s}^{-1}$). The electrochemical response of $[\text{Fe}(\text{CN})_6]^{3-/4-}$ displayed a peak-to-peak separation of $180 \pm 8 \text{ mV}$ (Gpt-CB-rPLA) and $240 \pm 6 \text{ mV}$ (CB-rPLA) compared to commercial AME ($740 \pm 10 \text{ mV}$), without any surface treatment. The filaments were used to create a 2,4,6-trinitrotoluene (TNT) detection platform with linear range of 5-20 and 5-100 $\mu\text{mol L}^{-1}$ for Gpt-CB-rPLA and CB-rPLA, respectively. The collector-detector device was applied for the analysis of a blast simulation. Finally, it is worth noting that the results obtained are without electrode treatment/activation, indicating that the rough surface of the additively manufactured electrode is an additional feature of the device for collecting explosive residues, simply by rubbing the additively manufactured platform on different surfaces in crime scenarios.

Keywords: recycled PLA, trinitrotoluene (TNT), 3D printing, electrochemical sensor, additive manufacturing, nitroaromatic compounds

Introduction

Additive manufacturing has brought significant impact to several different areas, including medicine, dentistry, food science, civil engineering, aerospace, chemistry, among others.¹⁻⁵ Within the chemistry area, electrochemistry can be highlighted with potential applications for (bio)sensors and energy storage devices aided by additive manufacturing technologies. One popular technology is fused deposition modeling (FDM) 3D printing, also called fused filament fabrication (FFF), in which desktop 3D printers deposit fused polymeric two-dimensional layers that generate the final 3D object after layer-by-layer deposition controlled by a computer aided design (CAD) file.⁶⁻⁸ FFF 3D

printing is widely accessible worldwide with inherent advantages including design freedom (from tiny to complex geometries), low generation of waste (feedstock rationally used), low cost fabrication, fast prototyping and use of printable biopolymers.^{7,9} FFF 3D printers and 3D pens can be found in chemistry laboratories to construct different accessories and equipment as well as for educational purposes.^{10,11} Another advantage is the low cost of polymeric filaments, typically polylactic acid (PLA) and acrylonitrile butadiene styrene (ABS) are commonly used due to their physical-chemical properties compatible with FFF 3D printing.¹² However, to perform electrochemical measurements using additively manufactured electrodes, conductive filaments are required, which can be found on the market with being ProtoPasta® and BlackMagic® the most used brands or can be manufactured in the laboratory.¹³ Lab-made filaments have been an interesting

*e-mail: munoz@ufu.br

Editor handled this article: Eduardo Carasek



strategy to adjust the composition of chemical modifiers, conductive agents, plasticizers, and other additives that can significantly improve the conductivity of the filaments and affect the electrochemistry of additively manufactured electrodes.¹⁴⁻¹⁷ Furthermore, the use of castor oil in the production of conductive filaments brings sustainability improvements as it is a biological phase plasticizer. In 3D printing, its function is to prevent the printer filament from breaking, causing print failures.¹⁸ But before 3D printing, castor oil was already used in various sectors such as pharmacological and medicinal, coatings and paints, fertilizers, lubricants, hydraulic fluids, soaps, waxes, biodiesel and others.¹⁹ Furthermore, its use has already been reported in studies, such as in the preparation of biochar to evaluate Pb^{II}, Cd^{II} and Cu^{II} ions,²⁰ as a basis for the synthesis of gold nanotubes-nanowires-polyurethane and polyethylene glycol²¹ and also, as a corrosion inhibitor.²²

On the other hand, although FFF 3D printers use rationalized filaments to obtain a 3D object, the constant use of polymeric filaments generates plastic residues. The application of circular economy in additive manufacturing is an essential trend which considers the use of recycled polymers to construct novel devices.^{18,23} In this context, conductive filaments made of recycled PLA loaded with different conductive carbon-based materials have been reported to develop electrochemical sensors for various detections, such as oxalate,²⁴ bisphenol A,²² caffeine in real samples of tea and coffee,²⁵ and also for detecting complementary DNA (cDNA) of the yellow fever virus,²⁶ among others. In these approaches, the authors employ thermal procedures in which the polymer is heated and melted in a sealed chamber with the conductive filler and a plasticizer. Interestingly, this process does not demand the use of toxic/dangerous organics solvents, making it more environmentally friendly.¹⁶ The addition of conductive carbon materials can enhance the electrochemical performance of the sensor compared to additively-manufactured electrodes (AMEs) built with commercially available conductive filaments. Although, these procedures construct interesting AMEs, the electrochemical activity of their printed electrodes in native form is poor with sluggish kinetics if compared to other conventional carbonaceous surfaces (glassy carbon, boron doped diamond, carbon paste, etc.) In this regard, some works reported different procedures of post printing pretreatment/activations to improve the electrochemical behavior of the AMEs.^{27,28} Activation protocols are applied in order to reduce the high amount polymer binder on electrode surface, exposing more conductive filler and/or increasing the porosity of AME surface. Several strategies have been proposed to enhance the electrochemical activity of AME surfaces.²⁹ These

protocols are able to enhance the voltammetric profile of inner sphere redox couples. However, these protocols are costly, time-consuming, and can generate chemical residues.²⁹ In this sense, the development of a disposable electrode that combines the benefits of 3D-printing technology and satisfactory electrochemical performance without the requirement of surface treatments has proven to be highly appealing. This approach also reduced the time and reagent costs (eco-friendly), being very attractive for sustainable development.

One area of forensic analysis that has garnered a lot of interest from several research groups is the creation of new analytical procedures for explosive detection.³⁰⁻³² Given that explosives are frequently employed in terrorist acts, this interest stems from the necessity to develop low-cost and portable methods to enhance public security. In the forensic scenario, the creation of analytical methods that facilitate the detection of trace level of explosive residues at the crime scene and furnish information to aid in the identification of suspects has been made possible by the application of chemical expertise in conjunction with portable instrumentation.^{33,34}

Herein, we demonstrate that a conductive filament composed of recycled PLA loaded with carbon black and/or graphite can be used to obtain a single electroanalytical device that presents two functions: a collector of solid residues and an electrochemical sensor of explosive residues. Importantly, the electrochemical device only requires a surface polishing before use to obtain smooth surface, which is a remarkable feature considering that most additively manufactured electrodes require additional surface treatment protocols.³⁵ As a proof-of-concept, the 3D-printed device was used to collect and detect residues of the explosive 2,4,6-trinitrotoluene (TNT) in post-explosion samples. Before its application, the electrochemistry of TNT was investigated on the additively manufactured device.

Experimental

Reagents and samples

Acetonitrile (99.8% v/v) was purchased from Vetec (Rio de Janeiro, Brazil). Hexaammineruthenium(III) chloride (98% m/m) was purchased from Sigma-Aldrich® (St. Louis, MO, USA). Potassium ferrocyanide(II) (99% m/m), potassium ferricyanide(III) (99% m/m) and hydrochloric acid were acquired from Labsynth (São Paulo, Brazil). Potassium chloride (98% m/m) from Dinâmica® (São Paulo, Brazil). Sodium hydroxide was obtained from AppliChem Panreac (Barcelona, Spain). TNT (>96% m/m) was obtained by a donation from Brazilian Federal Police (Uberlândia,

MG, Brazil) and its stock solution (20.0 mM) was prepared by dissolving their respective solids in acetonitrile. For the electrochemical detection of TNT, a standard solution of 1.0 mM was prepared by diluting an aliquot of the initial stock solution in 0.01 mM HCl (pH 2.00) supporting electrolyte. All solutions were prepared with highly purity deionized water (resistivity $\geq 18.2 \text{ M}\Omega \text{ cm}$, Millipore Direct-Q3, Bedford, MA, USA). Recycled PLA was acquired from Gianeco (Turin, Italy). Carbon Black (C65) from PI-KEM (Tamworth, U.K.) and graphite powder ($> 20 \mu\text{m}$) was obtained from Merck (Gillingham, U.K.)

Filament production from recycled material

Before use, recycled polylactic acid (rPLA) was dried at $60 \text{ }^\circ\text{C}$ for 2.5 h to remove any residual water in the polymer. The filament composition was prepared by adding appropriate amounts of PLA, carbon black and/or graphite, and 10% wt. of castor oil, used as a plasticizer. The compounds (rPLA, carbonaceous conductive materials and castor oil) were mixed with a mixer at 70 rpm at $190 \text{ }^\circ\text{C}$ for 5 min in a Thermo Haake Polydrive Dynameter fitted with A Thermo Haake Rheomix 600 (Thermo-Haake, Germany). The polymer compound was then left to cool at room temperature and subsequently extruded using a Filabot EX6 as described in a previous process.¹⁸ Two conductive filaments were developed both containing 60 wt.% rPLA and 10 wt.% castor oil. The difference is the composition of conductive material: the first filament only contains 30 wt.% carbon black (CB) while the second is composed of 18 wt.% carbon black and 12 wt.% graphite (Gpt). The filaments were named CB-rPLA and Gpt-CB-rPLA.

FFF printing of working electrodes and electrochemical measurements

The FFF technique was used to print the working electrodes and electrochemical cells. A Flashforge Dreamer NX 3D FFF printer equipped with 0.8 mm nozzle (São José dos Campos, São Paulo, Brazil) was used to manufacture the working electrodes. Briefly, a circular shaped electrode (78.5 mm^2) was printed at $215 \text{ }^\circ\text{C}$ and a bed temperature of $90 \text{ }^\circ\text{C}$. The printing parameters were set up in layer thickness of 0.18 mm, two perimeters in a horizontal orientation with 100% infill density and a constant printing perimeter speed of 70 mm s^{-1} . A GTMax 3D printer (São Paulo, Brazil) was used to print the electrochemical cells. This cell is composed by ABS (GTMax, São Paulo, Brazil) and more information about it is described by Cardoso *et al.*³⁵

Cyclic voltammetry (CV), square wave voltammetry (SWV), and electrochemical impedance

spectroscopy (EIS) measurements were performed at room temperature in the presence of dissolved oxygen, using a μ -AUTOLAB type III or a PGSTAT128N potentiostat/galvanostat (Metrohm Autolab BV, Utrecht, The Netherlands) connected to a microcomputer and controlled by NOVA software 2.1.6. A platinum wire and Ag|AgCl saturated with KCl were used as auxiliary and reference electrodes, respectively. All electrochemical measurements were performed in triplicate and the results were expressed as an average and their respective standard deviation. The working electrodes (CB-rPLA, Gpt-CB-rPLA and commercial CB-PLA) were used after simple mechanical polishing with different sandpapers (44.3 and $12.6 \mu\text{m}$, respectively) to obtain a smooth surface.

Electrochemical impedance spectroscopy (EIS) characterizations of the 3D printed electrodes were performed using frequency between 50 kHz and 0.01 Hz with an amplitude of 10 mV in the presence of 2.0 mM $[\text{Fe}(\text{CN})_6]^{4-/3-}$ in 0.1 M KCl solution, applying the half-wave potential ($+0.22 \text{ V vs. Ag|AgCl|KCl}_{(\text{sat.})}$). The Randles equivalent circuit was applied to fit the experimental data to acquire the charge transfer resistance (R_{ct}) between the 3D printed electrode working surface and the redox probe.

TNT detection was performed using SWV with conditions reported by Siqueira *et al.*¹³ The SWV parameters values were amplitude = 40 mV; step potential = -6 mV and frequency of 20 s^{-1} and supporting electrolyte was 0.01 mol L^{-1} HCl.

Physicochemical characterization

X-ray photoelectron spectroscopy analyses were carried out using an AXIS Supra (Kratos, U.K.), equipped with a monochromated Al X-ray source (1486.6 eV), operating at 225 W and a hemispherical sector analyzer. The operation is realized fixing transmission mode with a pass energy of 160 and 20 eV for survey and region scans, respectively. The collimator was operated in slot mode for an analysis area of at around $700 \times 300 \mu\text{m}$. The FWHM of Ag 3d5/2 peak using a pass energy of 20 eV was 0.616 eV. Scanning electron microscopy (SEM) images were acquired using a Supra 40VP Field Emission (Carl Zeiss Ltd., Cambridge U.K.) with an average chamber and gun vacuum of 1.3×10^{-5} and 1×10^{-9} mbar, respectively. Samples were mounted in aluminum SEM pin stubs (12 mm diameter, Agar Scientific, Essex, U.K.). A thin layer of Au/Pd (8 V / 30 s) was sputtered on electrode surface with SCP7640 from Polaron (Hertfordshire, U.K.) with the aim to improve the contrast of these images. The particle sizes of the irregularly shaped graphite powder, calculated from SEM images, (Figure S6, Supplementary Information (SI) section)

ranged from 1 to 20 μm , these values are in accordance with the information provided by the manufacturer. In contrast, carbon black powder particles are predominantly spherical in shape and range from 44 to 89 nm, which are in agreement with values reported in the literature.³⁶

Raman spectroscopy was performed on a DXR Raman microscope (Thermo Scientific Inc., Waltham, MA, USA) configured with a 532 nm laser and operated using OMNIC 9 software. Thermogravimetric analysis (TGA) was performed using a Discovery Series SDT 650 controlled by Trios software (TA Instruments, DA, USA). Samples were mounted in alumina pans (90 μL) and tested using a ramp profile (10 $^{\circ}\text{C min}^{-1}$) from 0-800 $^{\circ}\text{C}$ under N_2 (100 mL min^{-1}).

Study about contact angle

Images of the contact angle of the working electrode surface were captured using a smartphone mounted on a universal holder. These images were taken 10 s after the launch of a deionized water droplet onto the surface of the working electrode. Subsequently, the angle between the tangent drawn at the liquid-air interface of the water droplet and the surface of the electrode was measured ($n = 3$) using GeoGebra software.³⁷

TNT sampling and detection

TNT explosion simulation was carried out in the city of Uberlândia (Brazil, Minas Gerais) with the help of the Brazilian Federal Police. The explosion simulation was conducted on a metallic surface using a TNT paste and a chemical mixture of lead azide and nitropenta, as detonator. The 3D-printed circular-shaped electrodes were mechanically polished and then used to sample residual dust on the blast surface. Two forms of collection were evaluated: (i) collection by friction for one minute over a region of around 30 cm \times 20 cm and (ii) collection

point by point for fifty times covering a region of around 30 cm \times 20 cm (similar manner executed by forensic experts for residues collections using wet cotton swabs).

Subsequently, the additively manufactured sampler-electrode was positioned at the bottom of the additively manufactured printed cell (with a capacity of 10 mL) and 5 mL of supporting electrolyte (0.01 mol L^{-1} HCl) was added to perform SWV measurements. The blanks presented in the voltammograms were obtained before using the electrodes as collectors. Figure 1 depicts a scheme of the TNT sampling and detection.

Results and Discussion

Production and characterization of filaments

The manufacturing of bespoke conductive filaments from recycled PLA, castor oil (plasticizer), CB and/or graphite were carried out in the same way as previously reported.^{18,25} This methodology is an interesting approach to achieve flexible filaments with great electrochemical activity. Moreover, the mixing thermal step did not require any organic solvents as seen in other previous works.^{14,38}

Thermogravimetric analysis of the filaments (CB-rPLA and Gpt-CB-rPLA) and their constituents was performed. Analysis of the rPLA and produced filaments is important to comprehend the historical thermal stability of the polymer. Additionally, the TGA provides information regarding mass of conductive filler on each filament. From the TGA data, Figure 2a, the temperature for the onset of degradation for the CB-rPLA and Gpt-CB-rPLA filaments were calculated to be 268 ± 3 $^{\circ}\text{C}$ and 279 ± 5 $^{\circ}\text{C}$, respectively. This indicated that the inclusion of graphite within the filament improved the thermal stability. However, it should be noted in both cases, the conductive filament is less thermally stable than the individual constituents, with the rPLA providing an onset temperature of 327 ± 7 $^{\circ}\text{C}$ and the pure castor oil a temperature of 300 ± 7 $^{\circ}\text{C}$. The TGA data within

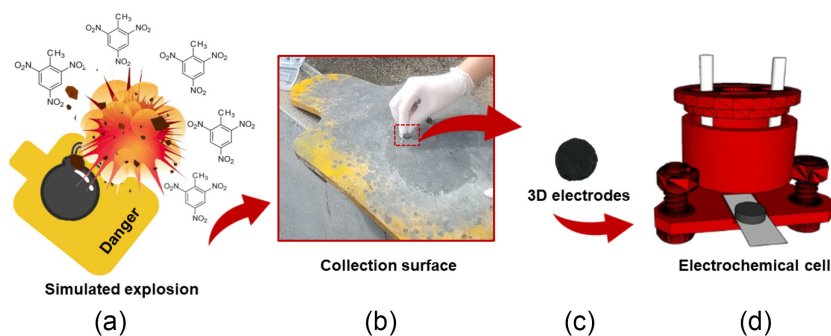


Figure 1. Schematization of sampling and detection of TNT residues: (a) simulated explosion performed by Federal Brazilian Police explosive experts; (b) real images showing the TNT collection on metal plate at which the TNT explosive was placed before explosion; (c) additively manufactured collector-electrode; and (d) additively manufactured-printed electrochemical cell ready to be assembled with the collector-electrode placed at the bottom of cell.

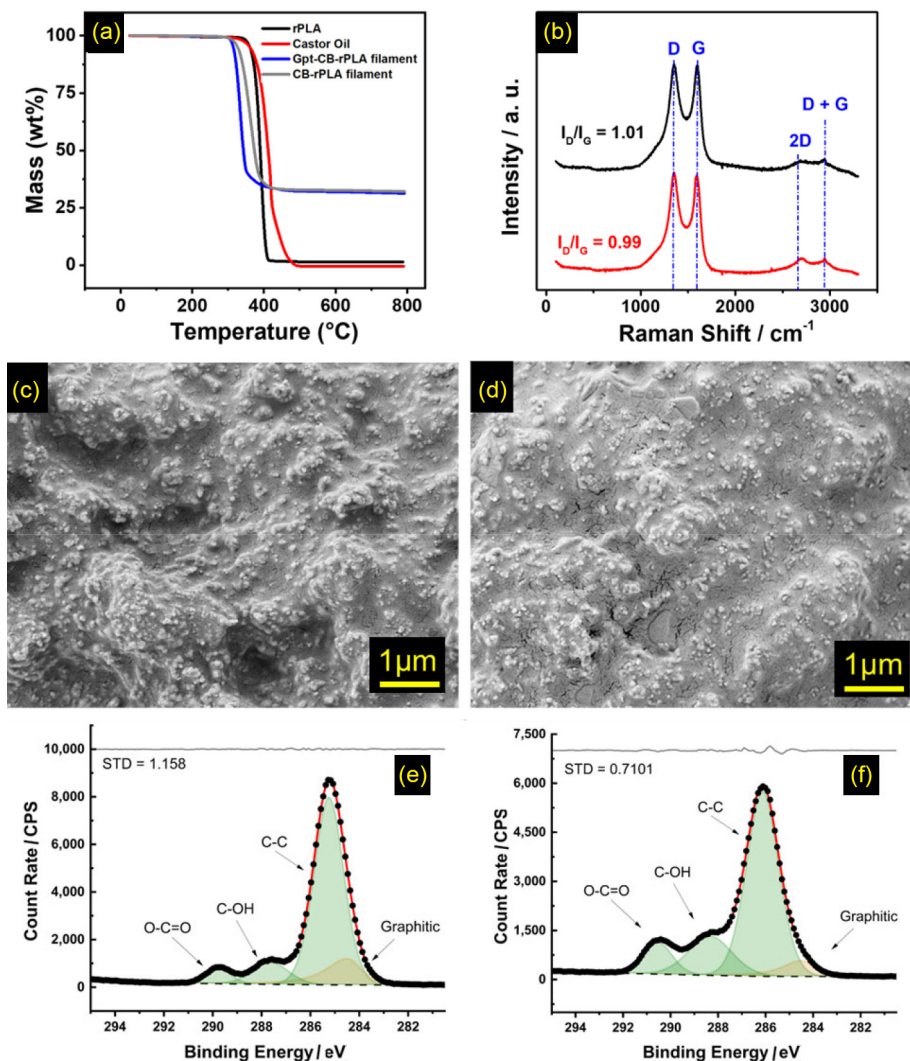


Figure 2. (a) Thermal gravimetric analysis of the recycled PLA (rPLA), castor oil, CB-rPLA and Gpt-CB-rPLA filaments. (b) Raman spectrum obtained for the CB/rPLA (black line) and Gpt-CB/rPLA (red line) electrodes surface. SEM surface images of the (c) CB/rPLA and (d) Gpt-CB/rPLA electrodes. XPS data for the (e) CB/rPLA and (f) Gpt-CB/rPLA electrodes.

Figure 2a was also used to calculate the exact amount of carbon filler present within the filaments after production. Through calculating the point at which the curves flatten after the degradation of rPLA and castor oil, and removing the residual 2 ± 1 wt.% remaining from the rPLA, the final filler masses were obtained to be 32 ± 1 wt.% and 31 ± 1 wt.% for the CB-rPLA and Gpt-CB-rPLA filaments, respectively.

Following characterization of the filament, it is important to establish the surface characteristics of the AMEs post-print as this is vital for the electrochemical performance. Figure 2b displays the Raman spectra obtained for the CB-rPLA (black) and Gpt-CB-rPLA (red), respectively. There are clear peaks present at 1338, 1572, and 2860 cm^{-1} , which are attributed to the characteristic D-, G-, and 2D-bands found within Raman spectra for graphitic structures. Through calculating the I_D/I_G ratio, the number

of defects and order can be implied. These were calculated to be 1.01 and 0.99 for CB-rPLA and Gpt-CB-rPLA, respectively, which indicates a higher number of defects and a less ordered structure, which is consistent with CB. SEM images, Figures 2c and 2d, confirm the presence of CB on the surface of the AMEs, where it can be clearly seen that spherical particulates of CB are protruding from the surface of the rPLA. In Figure 2d, a graphite flake can also be seen on the surface of the electrode, confirming the presence of graphite in this AME.

X-ray photoelectron spectroscopy (XPS) was then used to identify the surface functionalities present. Figures 2e and 2f present the XPS C 1s spectra obtained for both the CB-rPLA and Gpt-CB-rPLA AMEs. In both spectra three symmetric peaks are fitted and assigned to the O-C=O, C-O, and C-C functionalities, which are all found within the structures of PLA and castor oil. Due to the significantly

increased intensity for the C–C bonding peak, it can be inferred that there is castor oil present on the surface of the electrode, as if only PLA was present these peaks would be approximately equal intensities.^{18,25} To adequately complete the fitting of the C 1s spectra for both the CB-rPLA and Gpt-CB-rPLA AMEs, an asymmetric peak was required at 284.5 eV which is consistent with the X-ray photoelectron emission of graphitic carbon.^{39,40} This provides more evidence that there is indeed the presence of CB on the surface and the electrochemical performance of the AMEs should be good.

Study of interfacial phenomena

Figure S1 (SI section) illustrates the measured contact angle values for the 3D printed electrode surfaces. This parameter indicates the surface wettability.⁴¹ The values obtained for the Gpt-CB-rPLA and CB-rPLA electrodes were $78 \pm 1^\circ$ and $80 \pm 3^\circ$ before and $79 \pm 1^\circ$ and $82 \pm 2^\circ$ after sampling, respectively. Graphitic materials are known for their hydrophobic properties.^{39,42} However, the presence of PLA and the oxygenated groups on the electrodes reduces their hydrophobic nature towards water. Due to the higher PLA content in the electrodes, the materials exhibited contact angles close to 90° , demonstrating partial wettability of the surfaces. Comparatively, the contact angles observed on the Gpt-CB-rPLA and CB-rPLA electrodes indicate that their surfaces exhibit similar wettability characteristics before and after sampling applications.

Electrochemical characterization of AMEs

The electrochemical performance of the AMEs produced from recycled plastic material and carbon fillers, and the commercial filament was tested using a circular

design (Figure 1) to facilitate step of collecting real samples of the analyte of interest.

Initially, the electrodes made from recycled and commercial material were tested through cyclic voltammetry studies at varying scan rates ($5\text{--}500\text{ mV s}^{-1}$) using the near-ideal outer-sphere redox probe $[\text{Ru}(\text{NH}_3)_6]^{3+/2+}$ (1 mM in 0.1 M KCl), as shown in Figure S2 (SI section), to determine the heterogeneous electrochemical rate constant (k^0). It can be observed in Table 1, k^0 value obtained for Gpt-CB-rPLA electrodes (6.91 ± 0.58) $\times 10^{-3}\text{ cm s}^{-1}$ is higher than the CB-rPLA (5.31 ± 0.40) $\times 10^{-3}\text{ cm s}^{-1}$ and showed a significant improvement (ca. 2-fold) over the commercial filament (3.62 ± 0.38) $\times 10^{-3}\text{ cm s}^{-1}$. Additionally, the current intensities observed in Figure S1 is similar for both lab-made electrodes. However, the value decrease for electrodes printed with commercial filament.

The sensors were also tested with the inner-sphere probe $[\text{Fe}(\text{CN})_6]^{3-/4-}$ (2 mM in 0.1 M KCl) to further evaluate their electrochemical behavior (Figure 3 and Table 1). It is important to compare laboratory-made filaments tailored with the same weight percentage of conductive filler composed solely of carbon black to highlight the effect that graphite has on the system.²⁵ The cyclic voltammograms obtained at 50 mV s^{-1} are shown in Figure 3a. It is important to mention that the AMEs were not subjected to any surface activation protocol, only a surface polishing in order to remove lines of the printing (layer thickness). A notable improvement in terms of peak-to-peak separation (ΔE_p) and the ratio of anodic and cathodic signals was observed for the sensor containing graphite (180 ± 8) mV and I_{pa}/I_{pc} of 0.99 ± 0.02 compared to CB (240 ± 6) mV I_{pa}/I_{pc} of 1.11 ± 0.01 and a significant improvement over the commercial electrode (740 ± 10) mV and I_{pa}/I_{pc} of 1.10 ± 0.07 , indicating an effective enhancement in process reversibility and consequently in electrochemical

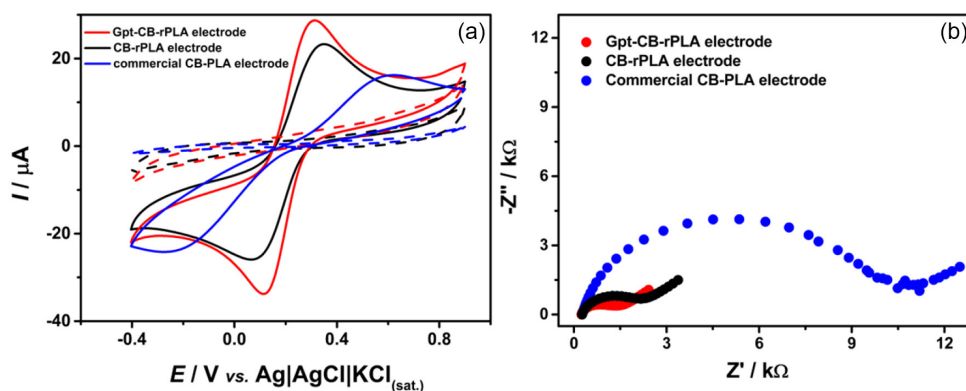


Figure 3. (a) Cyclic voltammograms recorded at $2\text{ mmol L}^{-1} [\text{Fe}(\text{CN})_6]^{3-/4-}$ in 0.1 M KCl solution, using different additively manufactured electrodes (the dashed lines refer the blank of analysis). CV conditions: scan rate (50 mV s^{-1}) and step potential (5 mV). (b) EIS Nyquist plots for additively manufactured electrodes acquired in the presence of $2\text{ mM} [\text{Fe}(\text{CN})_6]^{3-/4-}$ in 0.1 mol L^{-1} KCl solution applying a half-wave potential ($+0.22\text{ V vs. Ag|AgCl|KCl}_{(\text{sat.})}$). Frequency range between 0.1 to 50,000 Hz and signal amplitude of 10 mV. Each color refers a type of AMEs, as described below: CB-rPLA (black line), Gpt-CB-rPLA (red line) and commercial CB-PLA (blue line) electrodes.

Table 1. Comparison between electrochemical parameters, cathodic ($-I_{pc}$) and anodic (I_{pa}) peak currents intensities, peak-to-peak separation (ΔE_p), heterogeneous electron transfer (k^0), EIS charge transfer resistance (R_{ct}) for the non-treated CB-rPLA, Gpt-CB-rPLA and commercial CB-PLA electrodes

Parameter	Gpt-CB-rPLA	CB-rPLA	Commercial CB-PLA
$I_{pa}^{a,b} / \mu A$	27.9 ± 1.5	21.6 ± 1.9	8.7 ± 1.0
$-I_{pc}^{a,b} / \mu A$	28.2 ± 1.6	19.4 ± 1.7	7.9 ± 0.4
$I_{pa}/I_{pc}^{a,b}$	0.99 ± 0.02	1.11 ± 0.01	1.10 ± 0.07
$E_{pa}^{a,b,c} / mV$	300 ± 5	330 ± 3	570 ± 3
$E_{pc}^{a,b,c} / mV$	120 ± 3	90 ± 3	170 ± 8
$\Delta E_p^{a,b,c} / mV$	180 ± 8	240 ± 6	740 ± 10
$R_{ct}^a / k\Omega$	1.04 ± 0.05	1.81 ± 0.03	9.62 ± 0.03
$k^{0d} / (cm s^{-1})$	$(6.91 \pm 0.58) \times 10^{-3}$	$(5.31 \pm 0.40) \times 10^{-3}$	$(3.62 \pm 0.38) \times 10^{-3}$

^aThese results were performed using 2 mM $[Fe(CN)_6]^{3-/4-}$ redox probe in 0.1 M KCl solution. ^bThese CVs were performed at 50 mV s⁻¹. ^cvs. Ag(s)|AgCl(s)|KCl(sat.) reference electrode. ^dCalculated using 1 mM $[Ru(NH_3)_6]^{2+/3+}$ in 0.1 M KCl solution. CV scan rate study performed between 5 and 500 mV s⁻¹.

performance.^{24,38} In fact, XPS C1s spectrum analysis showed two oxygenated peaks (at 288 eV (C–OH) and 291 eV (O–C=O)) for Gpt-CB-rPLA with higher intensities when compared to XPS spectrum obtained for CB-rPLA electrodes. According the literature, the changes in C/O groups affected inner-sphere probes and can explain the enhancement in the electrocatalytic activity (shifted to less positive potentials, reduction in peak-to-peak separation) for Gpt-CB-rPLA electrodes.⁴³

As expected, the voltammetric profile for AMEs constructed with commercial filament is poor (ill-defined peaks) when using an inner-sphere probe since there are a large amount of PLA on surface (ca. 80 wt.%), requiring some activations procedures on surface to reduce the insulating material. On the other hand, the lab-made filament provided a satisfactory electrochemical activity (improvement in the reversibility). These results showed that the higher concentrations of conductive material (30 wt.%) for both lab-made filament) in the filament improve considerably the electrochemical performance of the AMEs without post-treatment after the printing since there are a considerable reduction in the quantities of polymer. Stefano *et al.*³⁸ also observed the same behavior when they manufactured a filament based on graphite (40 wt.%) and PLA. However, increasing the amount of conductive fillers in the composite filaments has the disadvantage of making the filament brittle⁴⁴ and, according to our experience, at more than 40% weight, the material could not be reliably fed into a 3D printer. Additionally, although Stefano *et al.*³⁸ managed to add a high load of conductive material, the peak-to-peak separation for $[Fe(CN)_6]^{3-/4-}$ redox pair was larger ($\Delta E_p = 264$ mV) when compared to CB-rPLA and Gpt-CB-rPLA electrodes, even if a smaller amount of conductive material (ca. 30 wt.%) was employed. It is important to emphasize that the use of plasticizer (castor oil) enhances the

printability of the filament and production of conductive filament by thermal process and is an interesting green approach to develop FFF materials. Finally, EIS was tested over frequencies ranging from 50,000 to 0.1 Hz in $[Fe(CN)_6]^{3-/4-}$ (2 mmol L⁻¹ in 0.1 mol L⁻¹ KCl), applying a half-wave potential of +0.22 V (vs. Ag|AgCl|KCl(sat.)) to determine the charge transfer resistance (R_{ct}).⁴⁵ Figure 3b presents the Nyquist plot obtained for all non-treated AMEs. Once again, electrodes produced from recycled material outperformed the commercial ones, with R_{ct} values of $1040 \pm 50 \Omega$ (Gpt-CB-rPLA) and $1810 \pm 30 \Omega$ (CB-rPLA) compared to $9620 \pm 280 \Omega$ (commercial CB-PLA). The results obtained from EIS and the k^0 values corroborate with the superior response of the laboratory-produced sensors compared to the commercial one, which indicate that the electron transfer was facilitated for CB-rPLA and Gpt-CB-rPLA electrodes.^{46,47}

Electrochemical determination of TNT by SWV

As proof-of-concept, the electrochemical behavior of 0.5 mmol L⁻¹ TNT explosive using non-treated AMEs, was investigated through cyclic voltammetric experiments in 0.01 M HCl solution. This experiment was carried out with previous conditions reported in the literature.¹³ The potential range studied was from -1.0 to 1.0 V (vs. Ag|AgCl|KCl(sat.)). As can be seen in Figure 4, ill-defined voltammetric profile (low current intensity) was achieved using additively manufactured CB-PLA electrodes while both electrodes printed from lab-made filaments improve considerably the electrochemical behavior in which is possible to discriminate three reduction processes (-0.35 , -0.57 , and -0.77 V vs. Ag|AgCl|KCl(sat.)) and a redox pair (at around $+0.14$ and $+0.41$ V vs. Ag|AgCl|KCl(sat.)). The cathodic peaks are related to reduction of three different nitro groups in the TNT structure. Firstly, the *ortho*-nitro with respect to methyl

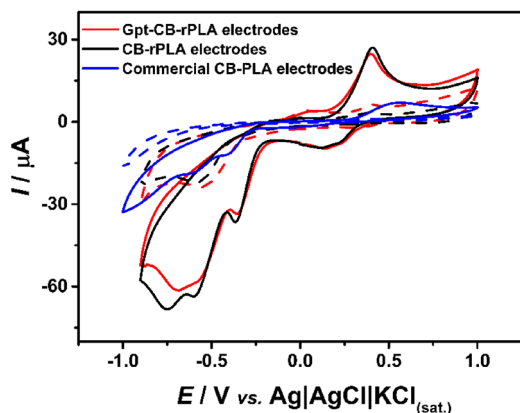


Figure 4. Cyclic voltammograms recorded at 0.5 mmol L^{-1} TNT in 0.01 M HCl solution, using 3D-printed (black line) CB-rPLA, (red line) Gpt-CB-rPLA and (blue line) commercial CB-PLA working electrodes. The dashed lines refer the blank of analysis. CV conditions: scan rate (50 mV s^{-1}) and step potential (5 mV).

group is reduced (at around $-0.35 \text{ V vs. Ag|AgCl|KCl}_{(\text{sat.})}$). Next, the reduction of another *ortho*-nitro group occurs (ca. $-0.57 \text{ V vs. Ag|AgCl|KCl}_{(\text{sat.})}$). Finally, the formation of last cathodic peak is related to reduction of nitro group in the *para* position. All nitro groups were reduced to hydroxylamine. The reaction in the redox pair is related to the oxidation of hydroxylamine and the reduction of the amine formed.^{13,48}

Calibration curves were constructed to assess the ability of Gpt-CB-rPLA, CB-rPLA, and commercial CB-PLA sensors to detect TNT at various concentrations (Figure 5), using SWV and the supporting electrolyte, according to previous published work. Table 2 summarized the results obtained for all 3D-printed sensors. As can be noted, both sensors were able to detect TNT at low concentrations, resulting in reduction peaks at potentials around -0.39 V and $-0.62 \text{ V vs. Ag|AgCl|KCl}_{(\text{sat.})}$ (Gpt-CB-rPLA), -0.36 V and $-0.58 \text{ V vs. Ag|AgCl|KCl}_{(\text{sat.})}$ (CB-rPLA), and -0.35 V and $-0.55 \text{ V vs. Ag|AgCl|KCl}_{(\text{sat.})}$ (commercial CB-PLA). However, the lab-produced filaments from recyclable material exhibited higher sensitivity (0.106 and $0.102 \mu\text{A L } \mu\text{mol}^{-1}$ for non-treated CB-rPLA and Gpt-CB-rPLA, respectively) compared to the commercial one ($0.041 \mu\text{A L } \mu\text{mol}^{-1}$). The electrode produced from CB and recycled PLA showed a linear range of $5\text{-}100 \mu\text{mol L}^{-1}$ ($r = 0.993$), with a limit of detection (LOD) of $3.42 \mu\text{mol L}^{-1}$ and the electrodes produced from graphite CB and rPLA presented two linear ranges ($5\text{-}20$ and $25\text{-}100 \mu\text{mol L}^{-1}$) with $\text{LOD} = 0.88 \mu\text{mol L}^{-1}$ while the electrode manufactured with commercial filament presented a linear range of $5\text{-}40 \mu\text{mol L}^{-1}$ ($r = 0.998$) and LOD of $1.55 \mu\text{mol L}^{-1}$. The limits of detection and quantification (LOD and LOQ, respectively) were estimated according to International Pure

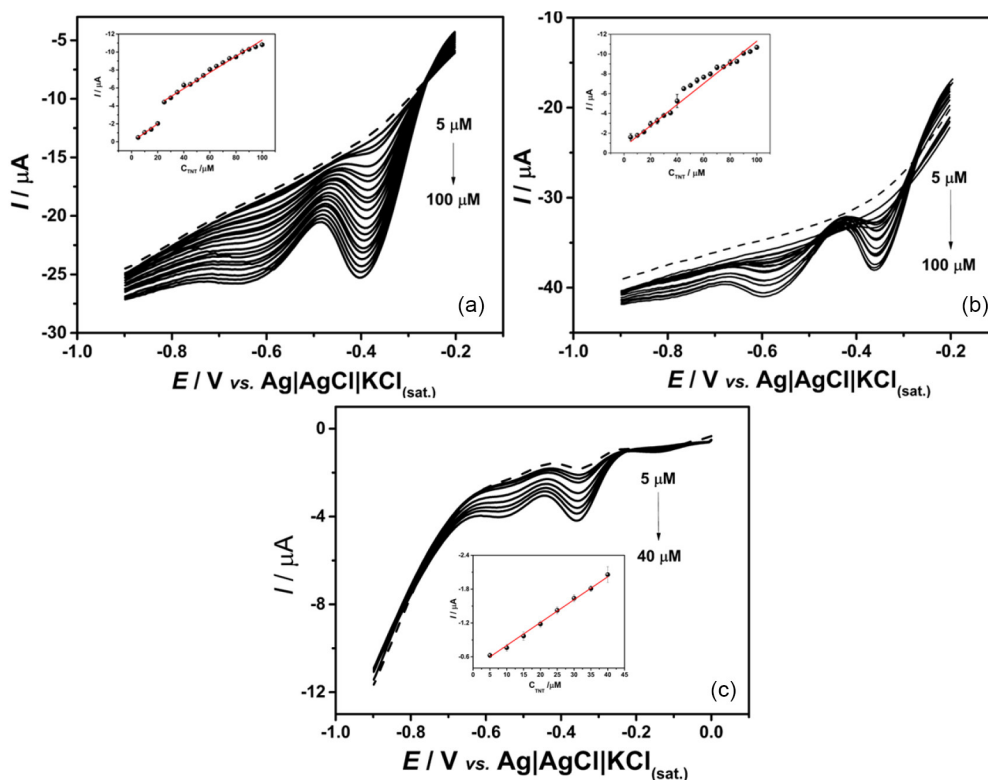


Figure 5. SWV for increasing of successive TNT concentrations (5 to $100 \mu\text{M}$) in 0.01 M HCl recorded at (a) Gpt-CB-rPLA, (b) CB-rPLA and (c) commercial CB-PLA electrodes and the respective calibration curve (insert graph). The dashed lines refer the blank of analysis. Step potential: -6 mV . Amplitude: 40 mV and frequency: 20 s^{-1} .

Table 2. Comparison of the analytical parameters obtained for TNT using 3D-printed Gpt-CB-rPLA, CB-rPLA and commercial CB-PLA working electrodes

Analytical parameter	Gpt-CB-rPLA	CB-rPLA	Commercial CB-PLA
R	0.998 ^a 0.996 ^b	0.993	0.998
R ²	0.995 ^a 0.991 ^b	0.987	0.996
Linear range / ($\mu\text{mol L}^{-1}$)	5-20 ^a 25-100 ^b	5-100	5-40
Slope / ($\mu\text{A L } \mu\text{mol}^{-1}$)	-0.102 ± 0.004^a -0.091 ± 0.003^b	-0.106 ± 0.002	-0.041 ± 0.009
Intercept / μA	0.026 ± 0.030^a -2.322 ± 0.121^b	-0.621 ± 0.121	0.396 ± 0.002
LOD / ($\mu\text{mol L}^{-1}$)	0.88 ^a 4.00 ^b	3.42	1.55
LOQ / ($\mu\text{mol L}^{-1}$)	2.94 ^a 13.30 ^b	11.40	5.17
RSD (inter-electrode, n = 5, 30.0 mM) / %	1.8	1.9	3.1
RSD (intra-electrode, n = 10, 30.0 mM) / %	1.9	2.6	4.0
RSD (inter-days, n = 5, 30.0 mM) / %	1.8	1.2	3.4

^aValues for the first linear range and ^bsecond linear range. R: correlation coefficient; R²: coefficient of determination; LOD: limit of detection; LOQ: limit of quantification; RSD: relative standard deviation.

and Applied Chemistry (IUPAC) recommendations,⁴⁹ where $\text{LOD} = 3.3\text{Sb/s}$ and $\text{LOQ} = 10\text{Sb/s}$, with Sb representing the standard deviation of ten blank measurements and s the slope of the calibration curve (Table 2). The difference in electrochemical response for the TNT explosive when using AMEs constructed with lab-made *versus* commercial filaments can likely be explained by the type of conductive filler present in the commercial filaments, as discussed in the previous section.

Although similar sensitivities were achieved for both lab-made electrodes, the material cost of producing conductive filaments with graphite, CB and PLA composite was £ 58.58 *per* kg, while the cost of manufacturing CB-rPLA was £ 83.06 *per* kg. Overall, commercial filament was more expensive than lab-made filaments in which is observed a price reduction of £ 24.28 and £ 48.76 for CB-rPLA and Gpt-CB-rPLA filaments, respectively.

The precision of the method was evaluated using both the lab-made and commercial sensors through an inter-electrode reproducibility study (n = 5) at a concentration of 30 μM TNT (see Figures S3B, S4B and S5B). The relative standard deviations (RSD) of the peak currents were 1.8, 1.9, and 3.1% for the GPT-CB-rPLA, CB-rPLA, and commercial electrodes, respectively, confirming the better reproducibility of the AMEs fabricated in the lab. Intra-electrode repeatability (n = 10) was also studied, where the same electrode was used throughout the day to determine 30 μM of TNT. The RSD values again confirmed the better efficiency of the recycled filaments (1.9% GPT-CB-rPLA and 2.6% CB-rPLA) compared to the commercial filament

(4.0%) (Figures S3D, S4D, and S5D). Based on the observed results, both electrodes can be effectively used as analytical sensors for TNT determination, as no fouling effect was observed. Finally, the inter-day repeatability of the electrodes was evaluated over five different days (n = 5) at 30 μM of TNT. RSD values of 1.8, 1.2, and 3.4% were obtained for the GPT-CB-rPLA, CB-rPLA, and commercial electrodes, respectively (Figures S3F, S4F, S5F). These results confirm good precision for TNT detection by AMEs produced with recycled PLA. It is worth noting that no degradation effect was observed during the studies, and therefore the electrodes were discarded when their thickness significantly decreased after numerous polishing sessions. Table 2 provides a summary of the RSD values obtained.

The analytical features of the AMEs produced using recycled PLA was compared with other electrochemical sensors reported for TNT detection. Table 3 lists these characteristics for comparison. The comparison shows that the obtained LOD values are not so low when compared with sophisticated platforms employing different chemical modifiers. On the other hand, they are well comparable with other low-cost electrochemical sensors, such as those based on PLA composites. However, the proposed 3D-printed device herein reported is the single one that employs recycled PLA and thus contributes to circular economy.

TNT detection in post-explosion samples

As the AMEs produced with the laboratory-produced filaments (Gpt-CB-rPLA and CB-rPLA) showed greater

Table 3. Comparison of the electrochemical sensors produced with others reported in the literature for TNT determination

Sensor	Analytical technique	Sample	LOD ^a / ($\mu\text{mol L}^{-1}$)	Reference
Fe ₃ O ₄ @Au/CA	SWV	tap water, Razan River water, and Persian Gulf water	0.0005	50
B-NCD	SWV	seawater	0.044	51
CdS nanoparticles	Amp	tap, river and lake water	0.001	52
MIPEDOT/LIG	DPV	river water, seawater and wastewater from the Wanquan River	0.009	53
GC/GNSs/pCAF	DPV	real sample assay for TNT	0.026	54
SPEs modified with TNT-specific peptides	EIS	–	low as 10 ⁻⁶	55
SPCE	DPV	river water	4.4 × 10 ⁻³	56
Graphene-PLA doped with diamond foil	DPV	–	0.4	57
GC/P(Cz-co-ANI)-Au _{nano}	SWV	military-purpose mixed explosives	0.11	58
PtPd-rGONRs/GCE	LASV	tap and lake water	0.0035	59
Gpt-PLA	SWV	tap, river and seawater	0.52 and 0.66	12
Gpt-CB-rPLA and CB-rPLA	SWV	post-explosion	0.88 3.42	this work

^aDifferent concentration unities were converted to $\mu\text{mol L}^{-1}$. Fe₃O₄@Au/CA: sensor constructed by modifying a graphite paste with Fe₃O₄-Au core-shell nanoparticles modified with cysteamine; B-NCD: boron-doped diamond electrode; MIPEDOT/LIG: electrochemical sensor based on dummy molecularly imprinted poly (3,4-ethylenedioxythiophene)/laser-induced graphene; GC/GNSs/pCAF: sensor was created by combining electrochemically reduced graphene nanosheets (GNSs)-through cyclic voltammetric reduction of a graphene oxide colloidal solution-with phosphate-stabilized poly-caffeic acid (pCAF) film-modified glassy carbon electrode (GCE); SPCE: screen printed carbon electrode; α -Al₂O₃/GCE: glassy carbon electrode modified with alumina; GC/P(Cz-co-ANI)-Au_{nano}: glassy carbon electrode modified with gold/poly(carbazol-aniline) nanoparticle film; PtPd-rGONRs/GCE: glassy carbon electrode modified with concave PtPd nanocubes anchored in graphene nanoribbons; SWV: square wave voltammetry; Amp: amperometry; DPV: differential pulse voltammetry; EIS: electrochemical impedance spectroscopy; LASV: linear adsorption stripping voltammetry.

electrochemical response than electrodes printed with the commercial filaments, they were used as a sampler in a TNT explosion simulation to test their applicability in real samples and their versatility as sample collectors. For this purpose, an explosion simulation was conducted on a metallic surface using a TNT paste and a chemical mixture of lead azide and nitropenta, as detonator with the help of Brazilian Federal Police. The electrodes were printed in a circular shape to facilitate movement during collection (Figure 1), using Gpt-CB-rPLA and CB-rPLA electrodes, and were directly used as collectors at the explosion site. Prior to this, they underwent mechanical polishing (for one minute), and blank measurements were conducted in a 0.01 M HCl supporting electrolyte. The same electrodes were used for collection, and two methods of collecting TNT were tested: one by friction (for one minute) and the other by point collection, where the electrode was placed and removed from the surface fifty times consecutively. In Figure 6, we showed the electrochemical response of 50 μM TNT standard solution, to facilitate the visualization of the TNT processes for each type of electrodes.

The friction collections of both electrodes (Figures 6a and 6c, for Gpt-CB-rPLA and CB-rPLA electrodes, respectively) demonstrate their effectiveness in detecting the presence of TNT in small quantities, as evidenced by

the characteristic reduction peak of TNT at around -0.36 V (vs. Ag|AgCl|KCl_(sat.)). On the other hand, the TNT sampling by point collection (Figures 6b and 6d) did not prove to be as effective as TNT sampling by friction, which could be attributed to the limited adhesion of the analyte on the electrode surface as well the short contact time between the electrode and the explosion surface.

Conclusions

This study showed the use of filaments made from graphite and carbon black with recycled PLA and castor oil as plasticizers for the production of additively manufactured electrodes for TNT detection. Electrodes manufactured in the laboratory presented analytical parameters with greater precision and reproducibility compared to commercial electrodes. Furthermore, they presented superior electrochemical response (lower resistance and greater sensitivity). They also offered cost benefits due to laboratory production. The cost of producing 1 kilogram of the mixture of graphite, carbon black and recycled PLA is £58.58, while carbon black and rPLA alone cost £83.06 and ProtoPasta® costs £107.34. The significant reduction in the production cost of Gpt-CB-rPLA is attributed to the fact that graphite powder is twelve times cheaper than carbon black.

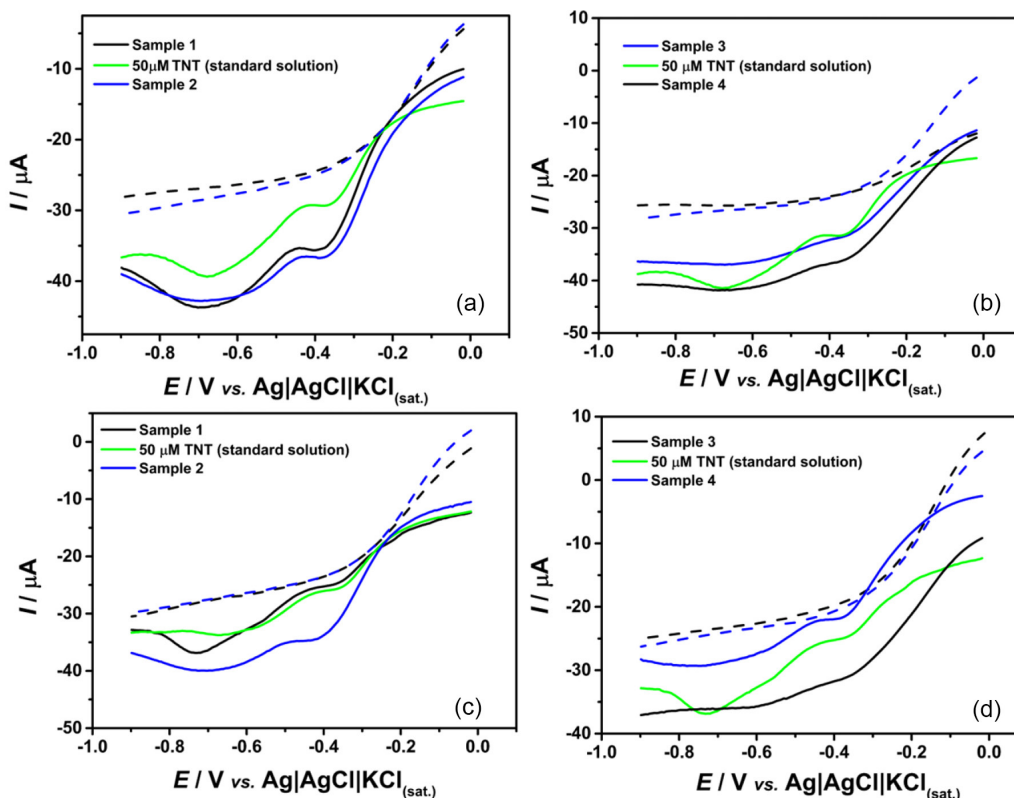


Figure 6. SWV responses for the blank (dashed lines) and TNT samples collected after simulated explosion with the help of Brazilian Federal Police (samples 1, 2, 3 and 4), using 0.01 M HCl. (a, b) Gpt-CB-rPLA and (c, d) CB-rPLA electrodes were used as collectors (samples 1 and 2 were obtained by friction while samples 3 and 4 point by point). The green line refers the SWV response for a standard solution of 50 μM TNT. SWV conditions: amplitude = 40 mV; step potential = -6 mV; frequency = 20 s^{-1} .

Additionally, we demonstrated that TNT can be detected using an additively manufactured cell with electrodes made from recycled material. Moreover, the electrodes printed with recycled PLA successfully functioned as direct TNT waste collectors. After passing the electrode over the explosion surface, it was mounted on the additively manufactured cell, and SWV scans confirmed the presence of the analyte. It is worth highlighting that electrodes did not require any electrochemical modification to achieve satisfactory detection, offering an added advantage for routine applications with the proposed dual-function device: collector/detector.

Supplementary Information

Supplementary information (Figures S1, S2, S3, S4, S5 and S6) is available free of charge at <http://jbcbs.sbq.org.br> as PDF file.

Acknowledgments

The authors are thankful to the Brazilian science foundation agencies CNPq (grants 405620/2021-7, 308392/2022-1, 408462/2022-1, 401977/2023-4, and

315838/2021-3), FAPEMIG (grants APQ-02067-23, RED-00120-23, and APQ-02391-22) and CAPES (financial code 001) for financial support.

Author Contributions

Maria M. C. Souza was responsible for data curation, writing original draft; Gilvana P. Siqueira for data curation, writing original draft; Raquel G. Rocha for data curation, writing original draft; Robert D. Crapnell for data curation, writing-review and editing; Mário H. P. Santana for supervision, formal analysis; Eduardo M. Richter for supervision, funding acquisition, writing-review and editing; Craig E. Banks for funding acquisition, writing-review and editing; Rodrigo A. A. Muñoz for conceptualization, supervision, funding acquisition, resources, project administration, writing-review and editing.

References

1. Pati, F.; Ha, D. H.; Jang, J.; Han, H. H.; Rhie, J. W.; Cho, D. W.; *Biomaterials* **2015**, *62*, 164. [Crossref]
2. Derossi, A.; Caporizzi, R.; Azzollini, D.; Severini, C.; *J. Food Eng.* **2018**, *220*, 65. [Crossref]
3. Huang, S. H.; Liu, P.; Mokasdar, A.; Hou, L.; *Int. J. Adv. Des. Manuf. Technol.* **2013**, *67*, 1191. [Crossref]

4. Gupta, M. K.; Meng, F.; Johnson, B. N.; Kong, Y. L.; Tian, L.; Yeh, Y.-W.; Masters, N.; Singamaneni, S.; McAlpine, M. C.; *Nano Lett.* **2015**, *15*, 5321. [Crossref]
5. Carrasco-Correa, E. J.; Herrero-Martínez, J. M.; Simó-Alfonso, E. F.; Knopp, D.; Miró, M.; *Microchim. Acta* **2022**, *189*, 173. [Crossref]
6. Bell, C.; *Maintaining and Troubleshooting Your 3D Printer*; Springer: New York, 2014, p. 3. [Crossref]
7. Erokhin, K. S.; Gordeev, E. G.; Ananikov, V. P.; *Sci. Rep.* **2019**, *9*, 20177. [Crossref]
8. Ambrosi, A.; Bonanni, A.; *Microchim. Acta* **2021**, *188*, 265. [Crossref]
9. Stefano, J. S.; Kalinke, C.; da Rocha, R. G.; Rocha, D. P.; da Silva, V. A. O. P.; Bonacin, J. A.; Angnes, L.; Richter, E. M.; Janegitz, B. C.; Muñoz, R. A. A.; *Anal. Chem.* **2022**, *94*, 6417. [Crossref]
10. Pinger, C. W.; Geiger, M. K.; Spence, D. M.; *J. Chem. Educ.* **2020**, *97*, 112. [Crossref]
11. Cardoso, R. M.; Castro, S. V. F.; Stefano, J. S.; Muñoz, R. A. A.; *J. Braz. Chem. Soc.* **2020**, *31*, 1764. [Crossref]
12. Silva, A. L.; Salvador, G. M. S.; Castro, S. V. F.; Carvalho, N. M. F.; Munoz, R. A. A.; *Front. Chem.* **2021**, *9*, 684256. [Crossref]
13. Siqueira, G. P.; Araújo, D. A. G.; de Faria, L. V.; Ramos, D. L. O.; Matias, T. A.; Richter, E. M.; Paixão, T. R. L. C.; Muñoz, R. A. A.; *Chemosphere* **2023**, *340*, 139796. [Crossref]
14. Foster, C. W.; Elbardisy, H. M.; Down, M. P.; Keefe, E. M.; Smith, G. C.; Banks, C. E.; *Chem. Eng. J.* **2020**, *381*, 122343. [Crossref]
15. Cardoso, R. M.; Kalinke, C.; Rocha, R. G.; dos Santos, P. L.; Rocha, D. P.; Oliveira, P. R.; Janegitz, B. C.; Bonacin, J. A.; Richter, E. M.; Munoz, R. A. A.; *Anal. Chim. Acta* **2020**, *1118*, 73. [Crossref]
16. Crapnell, R. D.; Kalinke, C.; Silva, L. R. G.; Stefano, J. S.; Williams, R. J.; Abarza Munoz, R. A.; Bonacin, J. A.; Janegitz, B. C.; Banks, C. E.; *Mater. Today* **2023**, *71*, 73. [Crossref]
17. Ciešlik, M.; Susik, A.; Banasiak, M.; Bogdanowicz, R.; Formela, K.; Ryl, J.; *Microchim. Acta* **2023**, *190*, 370. [Crossref]
18. Crapnell, R. D.; Arantes, I. V. S.; Whittingham, M. J.; Sigley, E.; Kalinke, C.; Janegitz, B. C.; Bonacin, J. A.; Paixão, T. R. L. C.; Banks, C. E.; *Green Chem.* **2023**, *25*, 5591. [Crossref]
19. Patel, V. R.; Dumancas, G. G.; Viswanath, L. C. K.; Maples, R.; Subong, B. J. J.; *Lipid Insights* **2016**, *9*, LPI.S40233. [Crossref]
20. Kalinke, C.; Mangrich, A. S.; Marcolino-Junior, L. H.; Bergamini, M. F.; *J. Hazard. Mater.* **2016**, *318*, 526. [Crossref]
21. Ganji, Y.; Kasra, M.; Kordestani, S. S.; Hariri, M. B.; *Mater. Sci. Eng., C* **2014**, *42*, 341. [Crossref]
22. Godavarthi, S.; Porcayo-Calderon, J.; Casales-Díaz, M.; Vazquez-Velez, E.; Neri, A.; Martínez-Gomez, L.; *Curr. Anal. Chem.* **2016**, *12*, 476. [Crossref]
23. Silva-Neto, H. A.; Duarte-Junior, G. F.; Rocha, D. S.; Bedioui, F.; Varenne, A.; Coltro, W. K. T.; *ACS Appl. Mater. Interfaces* **2023**, *15*, 14111. [Crossref]
24. Arantes, I. V. S.; Crapnell, R. D.; Bernalte, E.; Whittingham, M. J.; Paixão, T. R. L. C.; Banks, C. E.; *Anal. Chem.* **2023**, *95*, 15086. [Crossref]
25. Sigley, E.; Kalinke, C.; Crapnell, R. D.; Whittingham, M. J.; Williams, R. J.; Keefe, E. M.; Janegitz, B. C.; Bonacin, J. A.; Banks, C. E.; *ACS Sustainable Chem. Eng.* **2023**, *11*, 2978. [Crossref]
26. Kalinke, C.; Crapnell, R. D.; Sigley, E.; Whittingham, M. J.; de Oliveira, P. R.; Brazaca, L. C.; Janegitz, B. C.; Bonacin, J. A.; Banks, C. E.; *Chem. Eng. J.* **2023**, *467*, 143513. [Crossref]
27. Abdalla, A.; Patel, B. A.; *Annu. Rev. Anal. Chem.* **2021**, *14*, 47. [Crossref]
28. Glowacki, M. J.; Cieslik, M.; Sawczak, M.; Koterwa, A.; Kaczmarzyk, I.; Jendrzewski, R.; Szykiewicz, L.; Ossowski, T.; Bogdanowicz, R.; Niedzialkowski, P.; Ryl, J.; *Appl. Surface Sci.* **2021**, *556*, 149788. [Crossref]
29. Rocha, D. P.; Rocha, R. G.; Castro, S. V. F.; Trindade, M. A. G.; Munoz, R. A. A.; Richter, E. M.; Angnes, L.; *Electrochem. Sci. Adv.* **2022**, *2*, e2100136. [Crossref]
30. de Oliveira, L. P.; Rocha, D. P.; de Araujo, W. R.; Muñoz, R. A. A.; Paixão, T. R. L. C.; Salles, M. O.; *Anal. Methods* **2018**, *10*, 5135. [Crossref]
31. O'Mahony, A. M.; Wang, J.; *Anal. Methods* **2013**, *5*, 4296. [Crossref]
32. Yu, H. A.; DeTata, D. A.; Lewis, S. W.; Silvester, D. S.; *TrAC, Trends Anal. Chem.* **2017**, *97*, 374. [Crossref]
33. Steinfeld, J. I.; Wormhoudt, J.; *Annu. Rev. Phys. Chem.* **1998**, *49*, 203. [Crossref]
34. Salles, M. O.; Meloni, G. N.; de Araujo, W. R.; Paixão, T. R. L. C.; *Anal. Methods* **2014**, *6*, 2047. [Crossref]
35. Cardoso, R. M.; Mendonça, D. M. H.; Silva, W. P.; Silva, M. N. T.; Nossol, E.; da Silva, R. A. B.; Richter, E. M.; Muñoz, R. A. A.; *Anal. Chim. Acta* **2018**, *1033*, 49. [Crossref]
36. Mazzaracchio, V.; Tomei, M. R.; Cacciotti, I.; Chiodoni, A.; Novara, C.; Castellino, M.; Scordo, G.; Amine, A.; Moscone, D.; Arduini, F.; *Electrochim. Acta* **2019**, *317*, 673. [Crossref]
37. *Geogebra*, version 6.0.853, International Geogebra Institute (IGI), 2024. [Link] accessed in September 2024
38. Stefano, J. S.; Guterres e Silva, L. R.; Rocha, R. G.; Brazaca, L. C.; Richter, E. M.; Abarza Muñoz, R. A.; Janegitz, B. C.; *Anal. Chim. Acta* **2022**, *1191*, 339372. [Crossref]
39. Gengenbach, T. R.; Major, G. H.; Linford, M. R.; Easton, C. D.; *J. Vac. Sci. Technol., A* **2021**, *39*, 013204. [Crossref]
40. Blume, R.; Rosenthal, D.; Tessonnier, J.; Li, H.; Knop-Gericke, A.; Schlögl, R.; *ChemCatChem* **2015**, *7*, 2871. [Crossref]
41. Huhtamäki, T.; Tian, X.; Korhonen, J. T.; Ras, R. H. A.; *Nat. Protoc.* **2018**, *13*, 1521. [Crossref]

42. Camargo, J. R.; Andreotti, I. A. A.; Kalinke, C.; Henrique, J. M.; Bonacin, J. A.; Janegitz, B. C.; *Talanta* **2020**, *208*, 120458. [Crossref]
43. Richter, E. M.; Rocha, D. P.; Cardoso, R. M.; Keefe, E. M.; Foster, C. W.; Munoz, R. A. A.; Banks, C. E.; *Anal. Chem.* **2019**, *91*, 12844. [Crossref]
44. Tully, J. J.; Meloni, G. N.; *Anal. Chem.* **2020**, *92*, 14853. [Crossref]
45. Randviir, E. P.; Banks, C. E.; *Anal. Methods* **2013**, *5*, 1098. [Crossref]
46. Olivé-Monllau, R.; Esplandiú, M. J.; Bartrolí, J.; Baeza, M.; Céspedes, F.; *Sens. Actuators, B* **2010**, *146*, 353. [Crossref]
47. Lazanas, A. C.; Prodromidis, M. I.; *ACS Meas. Sci. Au* **2023**, *3*, 162. [Crossref]
48. Chua, C. K.; Pumera, M.; Rulišek, L.; *J. Phys. Chem. C* **2012**, *116*, 4243. [Crossref]
49. Mocak, J.; Bond, A. M.; Mitchell, S.; Scollary, G.; *Pure Appl. Chem.* **1997**, *69*, 297. [Crossref]
50. Soltani-Shahrivar, M.; Afkhami, A.; Madrakian, T.; *Talanta* **2024**, *274*, 126041. [Crossref]
51. de Sanoit, J.; Vanhove, E.; Mailley, P.; Bergonzo, P.; *Electrochim. Acta* **2009**, *54*, 5688. [Crossref]
52. Salaria, K.; Mehta, N.; Krishna, C.; Mehta, S. K.; *Curr. Res. Green Sustainable Chem.* **2021**, *4*, 100166. [Crossref]
53. Zheng, C.; Ling, Y.; Chen, J.; Yuan, X.; Li, S.; Zhang, Z.; *Environ. Res.* **2023**, *236*, 116769. [Crossref]
54. Arman, A.; Sağlam, Ş.; Üzer, A.; Apak, R.; *Talanta* **2024**, *266*, 125098. [Crossref]
55. Zhang, D.; Jiang, J.; Chen, J.; Zhang, Q.; Lu, Y.; Yao, Y.; Li, S.; Logan Liu, G.; Liu, Q.; *Biosens. Bioelectron.* **2015**, *70*, 81. [Crossref]
56. Riedel, J.; Berthold, M.; Guth, U.; *Electrochim. Acta* **2014**, *128*, 85. [Crossref]
57. Lima, A. P.; Almeida, P. L. M. R.; Sousa, R. M. F.; Richter, E. M.; Nossol, E.; Munoz, R. A. A.; *J. Electroanal. Chem.* **2019**, *851*, 113385. [Crossref]
58. Sağlam, Ş.; Üzer, A.; Erçağ, E.; Apak, R.; *Anal. Chem.* **2018**, *90*, 7364. [Crossref]
59. Zhang, R.; Sun, C.-L.; Lu, Y.-J.; Chen, W.; *Anal. Chem.* **2015**, *87*, 12262. [Crossref]

Submitted: June 20, 2024

Published online: September 17, 2024